Appl. Phys. A (2016)122:118
DOI 10.1007/s00339-016-9648-z

Applied Physics A
Materials Science & Processing

INVITED PAPER

Photodisruption of a thin membrane near a solid boundary: an in vitro study of laser capsulotomy

G. Hawlina[1,2] · B. Drnovšek-Olup[1,2] · J. Možina[3] · P. Gregorčič[3]

Received: 13 October 2015 / Accepted: 20 January 2016

Abstract A Nd:YAG laser photodisruption is a well-established tool for intraocular surgery, such as treatment of posterior capsule opacification that affects the visual function. During the intraocular procedure, called laser capsulotomy, the excitation pulse is focused several times just behind the posterior capsule and intraocular lens to create the central opening in the opacified capsule. We built an in vitro experiment to (1) clarify the influence of the distance between the intraocular lens and the posterior capsule on the total pulse energy required for the capsulotomy, and (2) investigate the main mechanisms responsible for the posterior capsule opening. In our in vitro model, different distances between the solid boundary (imitating an intraocular lens) and the membrane (imitating the posterior capsule) simulate different types of posterior capsule opacification. Our results show that procedure efficiency decreases by decreasing distance between the lens and the capsule. We also explain that for smaller distances between the pulse focus and the membrane, plasma and shock wave are responsible for the capsule disruption. Here, a risk of collateral damage significantly increases. On contrary, the membrane and the bubble jet disrupt the membrane, when pulse focus is moved away and the risk of intraocular lens damage decreases. However, the membrane disruption is not very effective, if it is placed near the solid boundary that inhibits the membrane jet.

✉ P. Gregorčič
peter.gregorcic@fs.uni-lj.si

[1] Eye Hospital, University Medical Centre Ljubljana, Grablovičeva 46, 1525 Ljubljana, Slovenia

[2] Faculty of Medicine, University of Ljubljana, Vrazov trg 2, 1104 Ljubljana, Slovenia

[3] Faculty of Mechanical Engineering, University of Ljubljana, Aškerčeva 6, 1000 Ljubljana, Slovenia

1 Introduction

Effective Nd:YAG laser photodisruption with nanosecond laser pulses and energies of few millijoules is a well-established tool for intraocular surgery, such as Nd:YAG capsulotomy for the treatment of posterior capsule opacification (PCO) or late-postoperative capsular bag distension syndrome (CBDS) [1, 2]. The PCO and CBDS are the most common postoperative complications of modern cataract surgery that affect the visual function [3, 4]. During Nd:YAG laser capsulotomy, the excitation pulse is focused just behind the intraocular lens and posterior capsule (typically 100–200 μm), as schematically shown in Fig. 1. Here, a high-intensity laser pulse induces an optical breakdown resulting in a microexplosion initiated by plasma formation [5–7]. The plasma expansion is followed by different laser-induced phenomena [8, 9], such as a shock wave and the cavitation bubble, which are responsible for posterior capsule disruption. When a cavitation bubble expands to its maximum volume, it starts to collapse due to the liquid pressure. Under suitable conditions [10, 11], the collapsing bubble develops a liquid jet which can be responsible for the posterior capsule disruption [6, 12]. In such a way, by a single pulse, the posterior capsule is disrupted in a small area around the focal point. In order to clear the visual axis and improve patient's vision, a central opening in the opacified posterior capsule is performed by several pulses that are focused at different positions most commonly forming a cross [2, 13]. On the other hand, the laser-induced phenomena are also responsible for unwanted collateral effects such as intraocular

Published online: 03 February 2016

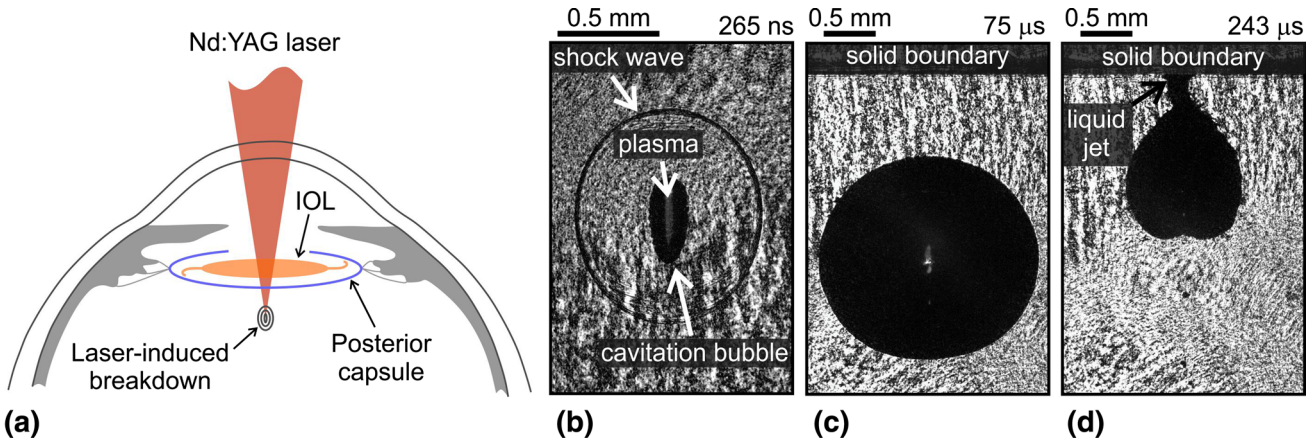

Fig. 1 **a** A schematic presentation of Nd:YAG laser capsulotomy. The laser pulse enters the eye through the cornea and is focused just behind the posterior capsule. **b** In the focus, the laser-induced breakdown is formed, causing a plasma, cavitation bubble, and shock wave. **c** When the bubble expands to its maximum volume, it starts to collapse, and under suitable conditions, it forms **d** a liquid jet, which hits the solid boundary (e.g., the intraocular lens)

lens damages [14] or damages of many delicate structures which are located very close to the breakdown region [15–17].

The PCO develops due to the lens epithelial cells remaining in the capsular bag after the cataract surgery [3]. Clinically, there are two basic morphological types of PCO: the fibrosis type and the pearl type, which have different cellular origins [18]. On the other hand, the visual function can also be affected by CBDS due to the accumulation of liquefied material in a closed space between the posterior capsule and the intraocular lens optic [4]. Various distances between intraocular lens and posterior capsule were recognized in different PCO types and CBDS, which could affect the total pulse energy needed to create capsulotomy of certain size [2]. We believe that this is related to bubbles' dynamics that depends on (1) the distance between the bubble's center and the boundary and (2) the boundary conditions. In the case of the laser capsulotomy, the boundary conditions depend on the PCO types—fibrosis and pearl type—or on CBDS, which differ by the mechanical properties (firmness) as well as by the distance between the posterior capsule (a thin membrane) and the intraocular lens (a solid boundary).

In our previous in vivo study [2], we have shown that both the PCO type and the distance between the intraocular lens and the posterior capsule significantly affect the total pulse energy needed to perform the capsulotomy. Since lower total pulse energy means fewer side effects, it is important to understand physical mechanisms that are responsible for these effects. However, we have found out that an in vitro experiment under more reproducible and controllable conditions should be designed to clarify the main mechanisms that are responsible for the posterior capsule disruption. Moreover, such an in vitro investigation would enable also to observe the isolated impact of different distances between the posterior capsule and the intraocular lens in different PCO types and CBDS. So, the main aim of this paper is a systematic study of the photodisruption of a thin elastic membrane near a solid boundary. We use a shadowgraphy and a laser-beam-transmission probe (LBTP) [19] for the investigation of membrane and solid boundary photodisruption at different distances between the boundary and the membrane. In such a way, we designed an in vitro model of an intraocular laser surgery, where the distance between the posterior capsule (a thin membrane) and an intraocular lens (a solid boundary) varies from full contact (i.e., 0 µm), as in the case of the fibrosis PCO type, to several hundreds of micrometers, as in the case of CBDS. The perforation of the membrane simulates the wanted effect of the posterior capsule disruption, which we observed and quantified by the size of the opening. On the other hand, the damages of the solid boundary represent the side effect that should be avoided during the laser capsulotomy and was, therefore, also recorded during our experimentation.

2 Materials and Methods

Figure 2 shows a sketch of the experimental setup. As an excitation source, we used a Q-switched Nd:YAG laser (Optotek, d.o.o., Slovenia), designed for intraocular photodisruption. The excitation laser has a wavelength of 1064 nm, pulse duration of 6 ns, and pulse energy up to 12 mJ. Its beam was focused into a vessel with distilled water. The focus position was placed above of an in vitro model that was placed in a two-dimensional (2D)

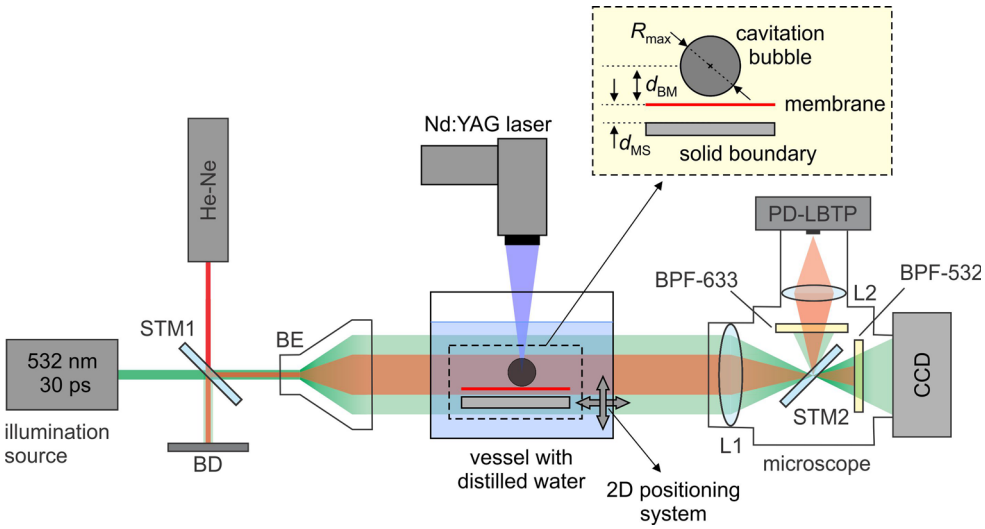

Fig. 2 Experimental setup

positioning system. An in vitro model of an intraocular laser surgery is schematically shown in the rectangle in Fig. 1. Here, we varied the distance between the bubble's center and the membrane (d_{BM}), as well as the distance between the membrane and the solid surface (d_{MS}). As a membrane, imitating the posterior capsule, we used an anterior capsule film from Kitaro Dry Lab cataract surgery training system (FCI Ophthalmics, Massachusetts, USA), while a polymethyl methacrylate (PMMA) rectangular cuboid of 1.5 mm thickness was used as an imitation of intraocular lens. The membrane and PMMA plate were located 35 mm under the water level to eliminate the free surface effects on the dynamics of the bubble.

A shadow photography [20, 21] was used to determine the distance between the bubble's center and the membrane. The experimental setup for shadowgraphy is quite straightforward: As an illumination source, we used a 30-ps, green laser (Ekspla, Lithuania, PL2250-SH-TH) led through a beam expander (BE), while the shadowgraph image was captured by a charge-coupled device (CCD) camera (Basler AG, Germany, scA1400-17fm, 1.4 Mpx). To acquire the whole bubble's dynamics from a single shot, we employed a LBTP [19] in our experiments. Here, a He–Ne is used as a CW illumination source. Its beam is coupled into the same path as for the shadowgraphic illumination by using a semi-transparent mirror (STM1), and it is led through the same BE as the illuminating pulse. Another semi-transparent mirror (STM2) is placed in a microscope to deflect the He–Ne beam on a lens (L2). After L2, the transmitted light is collected into an 1-GHz Si photodiode (PD-LBTP). A band-pass filter centered at 633 ± 10 nm (BPF-633) is placed in front of L2 to block green light, and vice versa, another band-pass filter centered at 532 ± 10 nm (BPF-532) is placed in front of CCD to block the light from He–Ne laser.

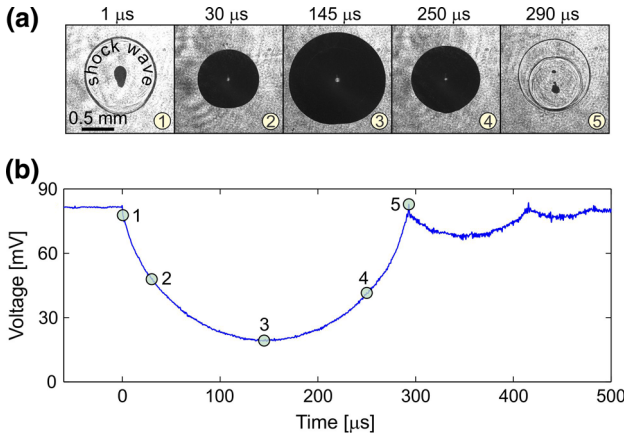

Fig. 3 **a** Typical shadowgraphic images. **b** Typical LBTP signal

Figure 3 shows typical shadowgraphic images (a) and typical LBTP signal (b). Here, the illuminating rays (from illuminating pulse or from a probe beam) that reach the bubble refract due to the refractive index gradients on its wall. This casts a shadow that can be visible on the screen [22]. Instead of the screen, we used a microscope equipped by a CCD camera and photodiode PD-LBTP. Immediately after the breakdown, a shock wave is visible in the shadowgraphic image (e.g., see the first image in Fig. 3a). A shock wave is emitted again at the end of the bubble's collapse [21] and is visible in fifth image in Fig. 3a. Typical events, captured by shadowgraphy, are marked by numbers on a typical LBTP signal (see Fig. 3b). Here, the transmitted probe power decreases by increasing bubble's radius and it reaches a minimum value at bubble's maximum volume (e.g., see mark 3 in Fig. 3a, b). In such a way, we were able to determine the maximum bubble's radius R_{max} by simultaneous use of a shadowgraphy and LBTP technique. The shadowgraphy was additionally used also

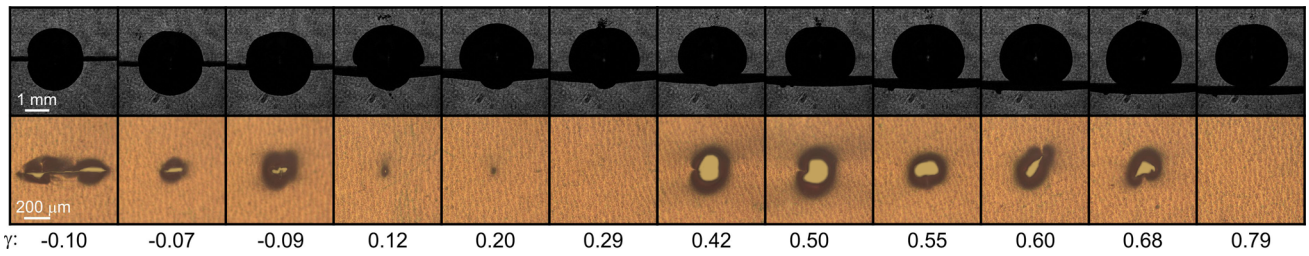

Fig. 4 *Second row* shows typical damages on a thin membrane, when the solid boundary is placed in infinite distance from the membrane. *First row* shows cavitation bubbles at its maximum volume for different distances d_{BM}. Dimensionless distance γ [e.g., see Eq. (1)] is shown on the *bottom* of each image

for measuring the distance d_{BM} between the bubble's center and the membrane.

We performed different series of the experiments with the following distances d_{MS} between the membrane and a PMMA plate: 0, 300 μm, and infinite (i.e., only a membrane was used). The distance between the membrane and a solid surface was achieved by using 100-μm-thick metal spacers. In such a way, we simulate different PCO types: fibrotic and pearl type, and CBDS, which we observed in our previous in vivo study [2]. At each d_{MS} distance, we performed three series of measurements. Here, in each series we changed the distance between d_{BM} the membrane and the bubble's center by moving the in vitro model.

After the disruption, the membrane and the PMMA plate were inspected under an optical microscope to recognize damages. The damages of the PMMA plate simulate the unwanted effect on an intraocular lens. On the other hand, the membrane damages represent the wanted effect at laser capsulotomy. Therefore, we acquired images of the damaged membrane by DSLR camera (Nikon, Japan, D90), and afterward, we measured their area and length by using ImageJ 1.50a program (Wayne Rasband, National Institutes of Health, USA).

3 Results and Discussion

Previous investigations [10, 11] have shown that the dynamical behavior of a bubble strongly depends on the dimensionless distance γ

$$\gamma = d_{BM}/R_{max}, \quad (1)$$

defined as the ratio between the distance d_{BM} and a maximum bubble's radius R_{max}. Therefore, all our results were analyzed and are presented as a function of dimensionless distance γ. In our case, we obtained an average maximum bubble's radius $R_{max} = 1.4$ mm for pulse energy of 12 mJ.

To simulate different PCO types, i.e., pearl and fibrotic type, and CBDS [2], we performed three series of experiments with different distances d_{MS} between the membrane and a solid surface. In the first series of our experiments, where we simulated CBDS, we used only a membrane, since in case of CBDS a large gap between the intraocular lens and a membrane occurs. Typical results are presented in Fig. 4. Here, the top images show the distances between the bubble's center (at its maximum radius) and the membrane. To acquire the bubble at its maximum radius, an appropriate time delay between the excitation and illumination pulses should be used. This delay was determined by a simultaneous use of a LBTP. The damages of the membrane for each particular dimensionless distance γ (given at the bottom of each image) are shown under the shadowgraphic images.

In the case of a membrane without a solid boundary (simulating CBDS), the size of the membrane damage decreases by moving a bubble from $\gamma = -0.10$ to 0.20 and there is no damage at $\gamma = 0.29$ (see sixth image in Fig. 4). However, the membrane is damaged again for $\gamma = 0.42$–0.68. For $\gamma \geq 0.79$, we did not observe any damage, which is in a concordance with the results obtained by other authors [12, 23, 24] who studied the effects of a cavitation bubble on an elastic membrane. Different regions of membrane damages reveal that several mechanisms are responsible for membrane perforation. We believe that for the dimensionless distances between -0.1 and 0.2, laser-induced plasma and shock wave create the hole in a membrane. Moreover, we observed a significantly larger damage for negative γ, as is clearly visible from the first three images in Fig. 4. The main reason for this may lie in the fact that in this case the plasma is induced "inside" the membrane and its expansion causes a significant damage. On the other hand, when laser focus moves away from the membrane, only small effect of plasma damage is obtained and the plasma-induced damage completely disappears for $\gamma > 0.20$.

Brujan et al. [24, 25] have shown that in the case of a bubble that oscillates near an elastic membrane, two jets can develop: (1) the jet caused by the bubble's collapse and (2) the jet that is created by the rebound of the deformed membrane. Their results show that the jet, induced by membrane deformation, appears for $\gamma < 0.5$ and it

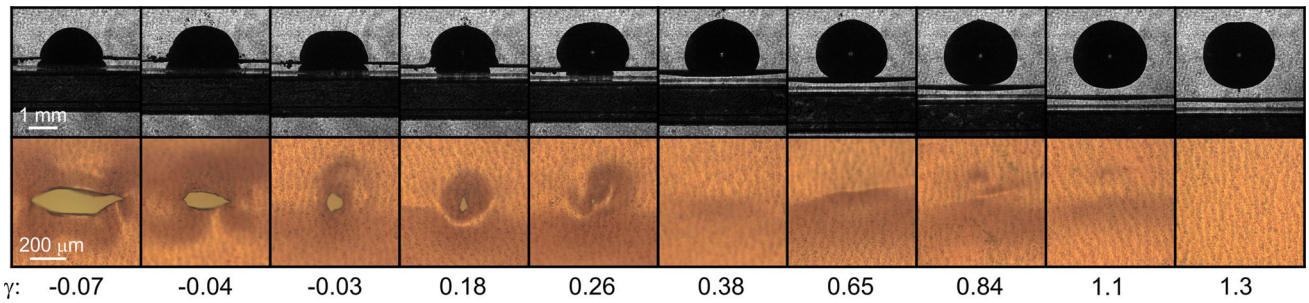

Fig. 5 Typical damages on a thin membrane (the *second row*) for the case when the membrane is placed 300 μm above a PMMA plate (*solid boundary*) as a function of dimensionless distance γ. The cavitation bubbles at its maximum volume are shown in the *first row*

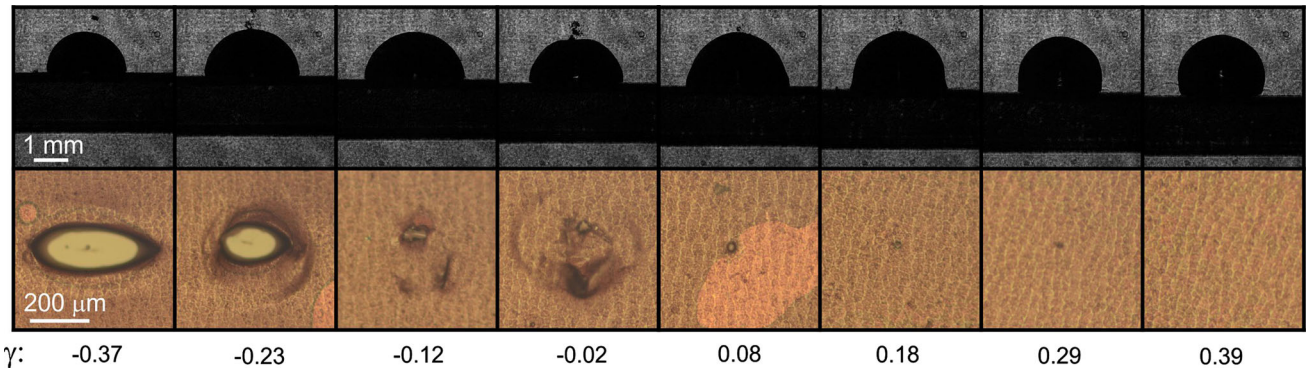

Fig. 6 Typical damages on a thin membrane (the *second row*) for the case when the membrane is in full contact with PMMA plate (*solid boundary*). The *first row* shows the cavitation bubbles at its maximum volume, while the dimensionless distance γ is presented on the *bottom* of each image

increases by decreasing γ. However, they have observed no penetration of the jet through the membrane for $\gamma < 0.2$ [22]. Additionally, they observed also a region, where the bubble's jet and the membrane's jet interfere with one another. Due to this reason, the jet induced by the membrane rebound inhibits the bubble's jet. A small region without a membrane damage that we observed around $\gamma = 0.29$ corresponds to a region where the laser focus is too far away from a membrane for plasma-induced damage. On the other hand, at this distance, the both jets interfere with one another and, consequently, no membrane damage appears or only a very small damage in a membrane is generated. On the contrary, for $\gamma = 0.42$–0.68, liquid jets that develop due to the bubble's collapse and the membrane deformation are responsible for the membrane disruption.

Typical images simulating the pearl type of the PCO are presented in Fig. 5. In this case, the membrane is 300 μm above the PMMA plate that simulates an intraocular lens. Here, we varied dimensionless distance γ from -0.07 to 2. However, we have not observed any damage on the PMMA plate within these distances. The main reason is that PMMA plate was too far away from a membrane (300 μm equals $\gamma = 0.21$ in our experiments) and plasma was not able to reach it. In this case, we observed a hole in a membrane only for $\gamma = -0.07$–0.26. Here, the plasma, shock wave, and the membrane jet represent the main mechanisms that open the capsule in the case of the pearl PCO type. For $0.38 \leq \gamma \leq 1.1$ only a fold, without any hole, is observed on the membrane. The fold is probably caused by a liquid jet that develops during the bubble's collapse. However, in this case the boundary conditions are different as in the case, when the bubble oscillates near a membrane without any solid boundary. Since the membrane deformation is limited by the presence of a solid boundary, the membrane jet is less pronounced as in the case of a membrane without a solid boundary. Therefore, it is not able to disrupt the membrane placed 300 μm above the solid surface. For $\gamma \geq 1.3$, we have not observed any damages on a membrane. From these results, it can be concluded that in the case of the pearl type of PCO, the focus of the excitation pulse should be precisely positioned just behind the posterior capsule to open the capsule without damaging an intraocular lens.

We simulated the fibrotic type of the PCO by a membrane that was in a full contact with a PMMA plate. Typical images for this case are presented in Fig. 6. We observed the hole in a membrane for $\gamma \leq 0.29$. However,

for negative γ we observed also damages of PMMA plate. In clinical practice, these damages should be avoided, since damaged intraocular lens can cause glare and worsen visual acuity after procedure [26]. So, in clinical practice, excitation pulse focus must be placed around $\gamma = 0$. However, in this position the size of the membrane damage for fibrosis PCO type is significantly smaller than at the same position in case of the CBDS and pearl PCO type. This explains our previous results obtained in an in vivo study [2] showing that a higher total pulse energy is required to perform capsulotomy in the case of fibrosis type, as in the case of CBDS or a pearl type. From the presented in vitro results, it can be concluded that the distance between the intraocular lens and the posterior capsule influences the total pulse energy that is required to perform the laser capsulotomy. The main reason lies in the fact that the presence of the solid boundary inhibits the jet that is developed due to the membrane deformation.

To obtain quantitative results of our experiments, we measured the length and the area of the damages, presented in Figs. 4, 5, and 6. The results of quantitative analysis are presented in Figs. 7 and 8. Figure 7 shows damage length as a function of dimensionless distance, while damaged area as a function of γ is shown in Fig. 8. Both, length and area are clinically important, since larger area in combination with longer damage means smaller amount of laser pulses (and consequently lower total pulse energy) that are needed to perform the laser capsulotomy. Lower total pulse energy decreases the probability for the unwanted side effects and makes ophthalmological procedure more effective and safer.

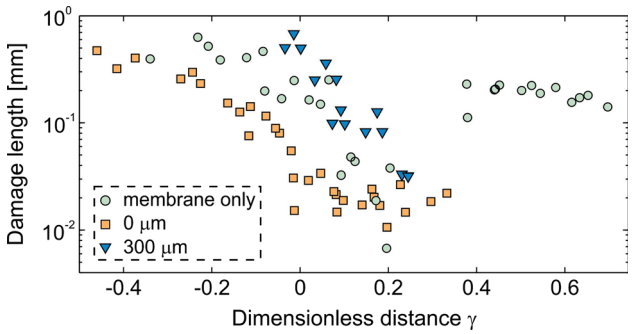

Fig. 7 Length of membrane damage as a function of dimensionless distance

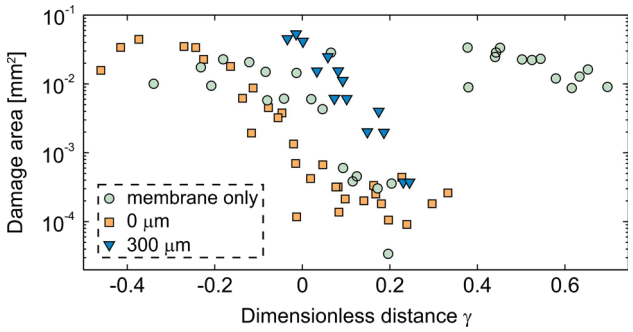

Fig. 8 Area of membrane damage as a function of dimensionless distance

From the results in Figs. 7 and 8, it can be concluded that four specific regions of dimensionless distance appear. In the first region defined by $\gamma < 0.2$, the damage dimensions exponentially decrease by increasing distance. In this region, the main mechanisms of membrane disruption are plasma and shock wave. They significantly disrupt the membrane. The second region occurs for $0.2 < \gamma < 0.4$. Here, the membrane is perforated in a very small area or its damage completely disappears. The reason lies in the fact that in this (second) region, the plasma is not able to perforate the membrane, since the focus is to far away; on the other hand, in this region the membrane jet inhibits the jet developed during the bubble's collapse. In the third region, limited by $0.4 < \gamma < 0.7$, the main damage mechanisms are liquid jets that develop due to the membrane deformation and the bubbles collapse. However, the third region exists only in the case when a membrane is not placed near a solid boundary (the circles in Figs. 7, 8). In the opposite case, if the membrane is around 300 µm above the solid boundary, only folds (without any hole) appear on the membrane or, if this distance is even smaller, the third region does not exist at all, as is visible from the squares and the triangles in Figs. 7 and 8. This leads to conclusion that the jet developed by the membrane deformation is the main mechanism of the membrane perforation. In the case of the presence of a solid boundary, the membrane deformation is limited, resulting in disappearing damages of the capsule. These findings are in consistence with our previous in vivo results [2], where we found out that lower total pulse energy is expected for a larger distance between intraocular lens and posterior capsule. The fourth region, i.e., a region without membrane damage, begins at $\gamma > 0.7$, which is consistent with results presented elsewhere [12, 23, 24].

4 Conclusions

We built an experimental setup that simultaneously employs a shadowgraphy and a laser-beam-transmission probe for in vitro investigations of the photodisruption of a thin elastic membrane with Nd:YAG laser-induced phenomena. In our in vitro model of an intraocular surgery, different distances between the solid boundary (imitating an intraocular lens) and the membrane (imitating the posterior capsule) simulate different PCO types and CBDS. To observe and analyze membrane damage length and area,

we used laser pulses that were focused at different distances from the membrane.

Our study revealed that several mechanisms are responsible for the membrane disruption. When the pulse focus is located near the membrane (i.e., $\gamma < 0.2$), plasma and shock wave are responsible for the capsule perforation. In this region, significant damages are obtained resulting in more effective treatment. However, a special care must be taken during the ophthalmic procedure in this region, since there is a risk of unwanted intraocular lens damage. The risk of collateral damage increases by decreasing distance between the posterior capsule and the intraocular lens. On the other hand, for distances $0.4 < \gamma < 0.7$ liquid jets that develop during the membrane rebound or the bubble's collapse are responsible for the membrane photodisruption. In this region, there is no risk of intraocular lens damage. Nevertheless, this region is not very effective for the case, when the posterior capsule is placed near the intraocular lens (i.e., if the distance between the membrane and the lens is <300 μm), since the lens inhibits the development of the membrane jet.

Our results explain that the distance between the posterior capsule and an intraocular lens is probably one of the most important factors that affect the total pulse energy needed to create capsulotomy in different PCO types in clinical practice. The size of the membrane damage is more pronounced at higher distances between the solid boundary and the membrane. Therefore, it can be concluded that the lower number of pulses is expected to create capsulotomy of a certain size for a larger distance between the posterior capsule and the intraocular lens.

References

1. C. Billotte, G. Berdeaux, J. Cataract. Refract. Surg. **30**, 2064 (2004)
2. G. Hawlina, D. Perovšek, B. Drnovšek-Olup, J. Možina, P. Gregorčič, BMC Ophthalmol. **14**, 131 (2014)
3. E.J. Hollick, D.J. Spalton, P.G. Ursell, M.V. Pande, Br. J. Ophthalmol. **82**, 1182 (1998)
4. K. Miyake, I. Ota, S. Ichihashi, S. Miyake, Y. Tanaka, H. Terasaki, J. Cataract Refract. Surg. **24**, 1230 (1998)
5. A. Vogel, W. Hentschel, J. Holzfuss, W. Lauterborn, Ophthalmology **93**, 1259 (1986)
6. A. Vogel, M.R. Capon, M.N. Asiyo-Vogel, R. Birngruber, Invest. Ophthalmol. Vis. Sci. **35**, 3032 (1994)
7. A. Vogel, S. Busch, U. Parlitz, J. Acoust. Soc. Am. **100**, 148 (1996)
8. P. Gregorčič, R. Petkovšek, J. Možina, G. Močnik, Appl. Phys. A **93**, 901 (2008)
9. A. Vogel, Phys. Med. Biol. **42**, 895 (1997)
10. Y. Tomita, A. Shima, J. Fluid Mech. **169**, 535 (1986)
11. A. Vogel, W. Lauterborn, R. Timm, J. Fluid Mech. **206**, 299 (1989)
12. U. Orthaber, R. Petkovšek, J. Schille, L. Hartwig, G. Hawlina, B. Drnovšek-Olup, A. Vrečko, I. Poberaj, Opt. Laser Technol. **64**, 94 (2014)
13. A. Gomaa, C. Liu, Eur. J. Ophthalmol. **21**, 385 (2011)
14. A. Trinavarat, L. Atchaneeyasakul, S. Udompunturak, J. Cataract Refract. Surg. **27**, 775 (2001)
15. D.S. Aron-Rosa, J.J. Aron, H.C. Cohn, J. Am. Intraocul. Implant. Soc. **10**, 35 (1984)
16. A. Vogel, *Optical Breakdown in Water and Ocular Media, and Its Use for Intraocular Photodisruption* (Shaker, Aachen, 2001)
17. P. Ranta, P. Tommila, T. Kivela, J. Cataract. Refract. Surg. **30**, 58 (2004)
18. D.J. Apple, K.D. Solomon, M.R. Tetz, E.I. Assia, E.Y. Holland, U.F. Legler, J.C. Tsai, V.E. Castaneda, J.P. Hoggatt, A.M. Kostick, Surv. Ophthalmol. **37**, 73 (1992)
19. P. Gregorčič, M. Jamšek, M. Lukač, M. Jezeršek, J. LA&HA **2014**, 14 (2014)
20. P. Gregorčič, M. Jezeršek, J. Možina, J. Biomed. Opt. **17**, 075006 (2012)
21. R. Petkovšek, P. Gregorčič, J. Appl. Phys. **102**, 044909 (2007)
22. G.S. Settles, *Schlieren and Shadowgraph Techniques* (Springer, Berlin, 2001)
23. A. Vogel, P. Schweiger, A. Frieser, M.N. Asiyo, R. Birngruber, IEEE J. Quantum Electron. **26**, 2240 (1990)
24. E.A. Brujan, K. Nahen, P. Schmidt, A. Vogel, J. Fluid Mech. **433**, 251 (2001)
25. E.A. Brujan, K. Nahen, P. Schmidt, A. Vogel, J. Fluid Mech. **433**, 283 (2001)
26. J.S. Lee, C.Y. Li, Y.C. Lin, S.Y. Chang, K.K. Lin, J. Cataract Refract. Surg. **29**, 621 (2003)